ARTICLE

Cerebrovascular Disease Progression in Patients With *ACTA2* Arg179 Pathogenic Variants

Arne Lauer, MD,* Samantha L. Speroni, BA,* Jay B. Patel, PhD, Ellen Regalado, MS, Myoung Choi, MD, Edward Smith, MD, Jayashree Kalpathy-Kramer, PhD, Paul Caruso, MD, Dianna M. Milewicz, MD, PhD, and Patricia L. Musolino, MD, PhD

Correspondence
Dr. Musolino
pmusolino@partners.org

Neurology® 2021;96:e538-e552. doi:10.1212/WNL.0000000000011210

Abstract

Objective

To establish progression of imaging biomarkers of stroke, arterial steno-occlusive disease, and white matter injury in patients with smooth muscle dysfunction syndrome caused by mutations in the *ACTA2* gene, we analyzed 113 cerebral MRI scans from a retrospective cohort of 27 patients with *ACTA2* Arg179 pathogenic variants.

Methods

Systematic quantifications of arterial ischemic strokes and white matter lesions were performed on baseline and follow-up scans using planimetric methods. Critical stenosis and arterial vessel diameters were quantified applying manual and semiautomated methods to cerebral magnetic resonance angiograms. We then assessed correlations between arterial abnormalities and parenchymal injury.

Results

We found characteristic patterns of acute white matter ischemic injury and progressive internal carotid artery stenosis during infancy. Longitudinal analysis of patients older than 1.2 years showed stable white matter hyperintensities but increased number of cystic-like lesions over time. Progressive narrowing of the terminal internal carotid artery occurred in 80% of patients and correlated with the number of critical stenoses in cerebral arteries and arterial ischemic infarctions. Arterial ischemic strokes occurred in same territories affected by critical stenosis.

Conclusions

We found characteristic, early, and progressive cerebrovascular abnormalities in patients with *ACTA2* Arg179 pathogenic variants. Our longitudinal data suggest that while steno-occlusive disease progresses over time and is associated with arterial ischemic infarctions and cystic-like white matter lesions, white matter hyperintensities can remain stable over long periods. The evaluated metrics will enable diagnosis in early infancy and be used to monitor disease progression, guide timing of stroke preventive interventions, and assess response to current and future therapies.

*These authors contributed equally to this work.

From the Departments of Neurology (A.L., S.L.S., P.L.M.) and Radiology (J.B.P., J.K.-K., P.C.), Massachusetts General Hospital, Harvard Medical School, Boston; Department of Internal Medicine (E.R., D.M.M.), McGovern Medical School, University of Texas Health Science Center at Houston; Department of Neuroradiology (A.L., M.C.), Goethe University, Frankfurt am Main, Germany; andDepartment of Neurosurgery (E.S.), Boston Children's Hospital, Harvard Medical School, Boston, MA.

Go to Neurology.org/N for full disclosures. Funding information and disclosures deemed relevant by the authors, if any, are provided at the end of the article.

Glossary

ACA = anterior cerebral artery; **AIS** = arterial ischemic strokes; **CL** = cystic-like white matter lesions; **CS** = critical stenosis on time of flight magnetic resonance angiography; **FLAIR** = fluid-attenuated inversion recovery; **ICA** = internal carotid artery; **IQR** = interquartile range; **IRB** = institutional review board; **MCA** = middle cerebral artery; **mCASS** = Cerebral Arteriopathy of Childhood Severity Score modified to include more than one territory and the posterior cerebral arteries; **MIP** = maximum intensity projection; **MGH** = Massachusetts General Hospital; **MRA** = magnetic resonance angiography; **SMDS** = smooth muscle dysfunction syndrome; **SWI** = susceptibility-weighted imaging; **T1W** = T1-weighted; **T2W** = T2-weighted; **T2*W** = T2*-weighted imaging; **TCD** = transcranial Doppler ultrasound; **TOF** = time of flight; **WMH** = white matter hyperintensities.

Heterozygous missense mutations disrupting arginine 179 (Arg179) in *ACTA2*, coding for smooth muscle specific isoform of α-actin, cause a syndrome characterized by disruption of the function of smooth muscle cells throughout multiple systems in the body.[1] Patients with smooth muscle dysfunction syndrome (SMDS) commonly present with congenital mydriasis, patent ductus arteriosus or aorto-pulmonary window, stroke, or aortic aneurysm or dissections.[2,3] Other disease manifestations include elastic arteries aneurysms, chronic lung disease, hypotonic bladder, gastrointestinal pathologies, and dysautonomia, including inability to adequately regulate blood pressure.[3]

Brain MRI radiologic findings include white matter hyperintensities (WMHs), arterial ischemic strokes (AIS), and steno-occlusive vasculopathy distinct from moyamoya disease due to lack of the classic network of basal collaterals,[4] straightening of the basal cerebral arteries,[5–7] and bilateral dilations of the elastic portions of the internal carotid artery (ICA).[8] Other brain anomalies include bending and hypoplasia of the anterior corpus callosum, flattening of the pons, and apparent "squeezing" of the cerebral peduncles.[9]

To date, determination of disease progression and risk of stroke needed to guide therapeutic interventions has been limited by the small number of patients and lack of longitudinal data in previously reported case series. Thus, we performed a retrospective review of the largest available cohort of patients with SMDS and characterized arterial and parenchymal lesions on MRI to further define the natural history of *ACTA2* Arg179-related cerebrovascular disease. Specifically, we quantified and evaluated changes in cerebral WMH volumes, number of cystic-like white matter lesions, ischemic lesions related to large artery occlusion, and changes in caliber and tortuosity of cerebral arteries.

Methods

Standard Protocol Approvals, Registrations, and Patient Consents

We performed a retrospective review of MRIs of patients with confirmed diagnosis of *ACTA2* (Arg179) pathogenic variants by genetic testing between 2002 and 2019. Participant data were de-identified with encrypted and password-protected storage. We analyzed demographic, clinical, and imaging data from patients recruited from the Montalcino Aortic Consortium registry housed at University of Texas Health Science Center at Houston and the Young Genetic Stroke Alliance registry housed at Massachusetts General Hospital (MGH), both approved by their respective institutional review board (IRB). New cases were added when patients were seen in these clinics or by self-referral to the registries. Inclusion criteria were a clinical syndrome consistent with *ACTA2* Arg179 and confirmed genetic testing. Outside investigators provided de-identified patient data after obtaining approval from their respective institutional review boards and consent from the patient or parents. Patients represented a wide geographic distribution from 5 countries: France, Germany, Australia, Israel, and 12 US states. Five patients had previously been included in the findings of Munot et al.[4]

A cohort of patients with pediatric stroke and no evidence of vasculopathy from the MGH Neonatal and Pediatric Neurovascular Disorders Registry (with IRB approval for consent waiver) were used as controls for the vessel imaging analysis.

Imaging

MRI Measures

Magnetic resonance studies of the brain were performed on various 1.5T/3.0T MRI units in various institutions around the world, using 8–64 channel head coils. At least 1 axial T2-weighted (T2W) sequence was available in each evaluated MRI protocol. The T2W sequences analyzed were axial fluid-attenuated inversion recovery (FLAIR) or axial T2W. FLAIR sequences were preferred for longitudinal quantitative analysis but only used if they were available throughout all visits. For quantitative analysis, sequences were transformed to the Neuroimaging Informatics Technology Initiative format. Diffusion- and susceptibility-weighted imaging was screened for acute ischemic or hemorrhagic lesions. Pre- and postcontrast T1-weighted (T1W) sequences were also reviewed whenever available. In addition, characterization of vessel abnormalities was performed on time of flight (TOF) magnetic resonance angiography (MRA) (echo time 2.4–7.0 ms, repetition time 18–44 ms, flip angle 15–25°, slice thickness 0.5–2.4 mm).

Lesion Burden and Pattern and Lesion Progression

Each MRI scan was reviewed by trained observers (a board-certified pediatric neuroradiologist [P.C.], a neuroradiologist

[A.L.], a neurologist [P.L.M.], and a research assistant trained in lesion quantification [S.L.S.]). The reviewers were blinded to patient characteristics (aside from obvious age-dependent degrees of myelination and other features directly implicated on imaging).

In young infants (age <6 months), scans were screened for presence of white matter abnormalities on T2W/T1W sequences and diffusion-weighted imaging following standard qualitative assessment as in routine clinical practice. In patients older than 12 months, cerebral lesions were quantified according to Standards for Reporting Vascular Changes on Neuroimaging (STRIVE).[10] We defined WMH as signal abnormality of any size in the supratentorial white matter on T2W imaging without cavitation/signal different from CSF. To quantify WMH and brain volumes we used a semi-automated, multistep protocol on axial FLAIR or T2W sequences modified from Chen et al.[11] using 3D-slicer software (slicer.org). With the exception of 3 patients who had bilateral, large AIS lesions that could not be reliably separated from other WMHs, any WMHs adjacent to cortical hyperintensities were considered AIS and excluded as part of the multistep protocol. After reviewing quantified WMH and to account for volumetric changes related to brain growth or tissue atrophy, which could bias the longitudinal data, scans were assessed for presence of WMH progression by comparing first and last available scans side by side and screened for involvement of additional areas of white matter (yes vs no).

Presence and number of AIS lesions, defined as T2W/FLAIR hyperintense lesions or fluid-filled cavities with signal similar to CSF involving cortical matter and subcortical and deep white matter following arterial territory patterns, were also evaluated. In addition, if blood product–sensitive imaging was performed (susceptibility-weighted imaging [SWI] or T2*-weighted imaging [T2*W]), sequences were screened for presence and number of both cerebral microbleeds and macro intracranial hemorrhages according to current consensus criteria. Susceptibility artifacts within AIS were considered secondary hemorrhagic lesions.

Cystic-like white matter lesions (CL), defined as smoothly edged, well-defined, round to ovoid with CSF signal were manually counted in T2W sequences. Lesions were not counted as CL if present in more than 2 axial planes without apparent change in diameter to avoid inclusion of mimics (flow-voids or prominent perivascular spaces imaged at a perpendicular angle to the course of the vessel). Irregularly shaped lesions of similar signal intensities were considered lacunar infarcts of presumed vascular origin and not CL.[10] Furthermore, MRI scans with available postcontrast sequences were assessed for the presence of abnormal contrast enhancement.

TOF MRAs were evaluated for anatomical variations and vessel abnormalities. Thirty-one pediatric age-matched patients with stroke without evidence of vasculopathy (stenosis, abnormal tortuosity, or dissection) were included as a comparative group. Previously described stereotypical vessel abnormalities include dilation of the petrous ICA segments and narrowing of the terminal intradural ICA segment. To evaluate changes over time, the largest bilateral diameters of the petrous ICA segments and the narrowest diameter of the terminal intradural ICA segment were quantified. We calculated the average of both sides unless TOF signal was missing due to ICA occlusion (n = 1). In this case, the contralateral diameter was used as the average for both sides.

In addition, vessels were screened for presence of critical stenosis (CS), defined as short- or long-segmented signal loss following the course of the vessel. Of note, this imaging-dependent definition does not imply a correlation with degree of stenosis or relative change in vessel caliber. To further evaluate degrees of global stenotic disease of the cerebral arteries feasible in the clinical setting, we performed a semi-quantitative scoring of segmental abnormalities of the cerebral arteries using the previously described focal Cerebral Arteriopathy of Childhood Severity Score modified to include more than one territory and the posterior cerebral arteries (mCASS).[12]

Each type of lesion assessment and quantification was performed by at least 2 readers independently. Measurements of WMH, CL, and vessel diameter quantification showed consistent results between readers (interrater agreement: Cohen κ = 0.9, 0.76, and 0.96, respectively). Final presence and number of CLs as well as binary WMH progression reads were determined by a consensus meeting and joint review of the discrepancies.

Automatic Vessel Tortuosity and Vessel Diameter Quantification

In a subset of patients (n = 9 SMDS and n = 5 age-matched nongenetic pediatric stroke patient controls), coronal slice maximum intensity projection (MIP) images were created from TOF. As a preprocessing step, all MIPs were resampled to isotropic pixel dimensions. Using 3D-Slicer, both the left and right ICA, middle cerebral artery (MCA), posterior cerebral artery, and anterior cerebral artery (ACA), along with the basilar artery, were manually segmented. A modified, fully automatic algorithm implemented in MATLAB was used to identify the centerlines of each vessel.[13] In short, we skeletonized each vessel mask and then ran a recursive search to find the longest uninterrupted path (which is assumed to be the centerline). For each vessel, a unitless tortuosity measurement was calculated, defined as the distance along the center line divided by the Euclidean distance between the endpoints of the vessel with a higher score implying a more tortuous vessel. The minimum and maximum diameter was tracked along each vessel. In addition, we extracted the angles between the ICA/MCA and the ICA/ACA.

Statistical Analysis

Variables treated as continuous are reported as mean ± SD or median with interquartile range (IQR) or the complete range.

Categorical variables are presented as numbers and percentages and were compared using χ^2 tests. Normally distributed continuous variables were compared using the unpaired *t* test and skewed distributed data were analyzed using the Mann-Whitney *U* test. Point-biserial and Pearson correlation were used to investigate associations between terminal/petrous ICA ratio and other imaging markers. Multivariate logistic regression analysis was used to determine which imaging markers were independently associated with AIS. The other chosen variables are considered potential risk factors based on published knowledge.[3] A binary logistic regression was used to evaluate the relation of AIS and degree of relative terminal ICA stenosis. One sample test of proportions was used to compare the actual vs the expected proportion of male patients in this cohort (0.51) with a 1-tailed *p* value of 0.05 indicating statistical significance. For all other tests, 2-tailed *p* values of 0.05 were used. Statistical analysis was performed using SPSS.22 for Macintosh software. Graphs were plotted using GraphPad Prism 8.3 software.

Data Availability

The data that support the findings of this study are available from the corresponding author upon request.

Results

Table 1 summarizes patient demographics and clinical data. A total of 113 MRI scans of 27 patients with SMDS performed between May 2002 and April 2019 were evaluated (median age at baseline in years [IQR] 2.07 [0.08–11.09], 20 female [74.1%]). Most patients were initially scanned because of symptoms (stroke, TIA, seizures, altered mental status, or headaches) and only 2 for screening of cerebral involvement following genetic diagnosis. No patient was scanned in the age range >6 months to 1.15 years. Follow-up imaging was available in 20 patients (74.1% with at least 2 available visits; of these, 22.2% had 3–5 visits, 25.9% had 6–10 visits, and 1 patient [3.7%] had >10 visits available; number of visits median [range] 3.5 [1–18]), with an average covered interval of 3.1 years (IQR 1.2–7.2 years). In this cohort, 19 patients (70%) had a confirmed p.Arg179His mutation and 7 patients (26%) a p.Arg179Cys mutation. One patient's specific amino acid substituting Arg179 was not known. More than 2/3 of patients (70.3%) were treated with antiplatelet drugs; 5 of these patients received additional anticoagulant treatment (63% before first scan and in 21% in the same year of stroke diagnosis).

Cerebrovascular Disease in Infants Includes Large Artery Vasculopathy and Internal Border Zone Infarctions

Eleven patients were scanned within the first 6 months of life (median age, d [range] 34 [2–179]). Cerebral artery abnormalities were already present in the youngest patient and characterized by dilated asymmetric carotid arteries in the petrous canal and cavernous sinus, short M1 segments (origin of the middle cerebral artery to its bifurcation), and abnormal straight course of the cerebral arteries (figure 1). All 11 patients showed white matter abnormalities that included patchy to confluent ring-like T1W-hyperintense/T2W-hypointense lesions of the supratentorial periventricular white matter consistent with early features of leukomalacia and focally to regionally enlarged ventricular systems (figure 2). In 5 of 11 patients, acute ischemic lesions established by areas of restricted diffusion were observed in the supratentorial deep white matter resembling the appearance of internal border zone infarcts. All 5 patients were scanned due to symptoms including seizures, dilated pupils with concern for herniation, and cardiac arrest perioperatively. The patient who cardiac arrest (due to an aortic dissection during surgery) showed extensive additional deep white matter and cortical infarctions. Four patients with long-term follow-up imaging showed WMH in the same areas of initial injury (figure 2).

Spatial and Temporal Characteristics of White Matter Lesions in Children and Young Adults

All patients aged 1.15–32.46 years showed patchy to confluent T2W hyperintensities of the periventricular white matter (median WMH volume, mL [IQR] 25.95 [16.82–53.55], % of whole brain volume 3.56% ± 2.19%, n = 19, figure 3, A–D). As observed in infants, these areas matched deep border zone white matter territories. Larger extension into the deep and subcortical white matter (without cortical injury) was seen in 8 patients. We observed limited cerebellar WMH in 4 patients (14.8%), which was best visualized on thin sliced coronal T2W imaging (figure 3C). Longitudinal observation revealed no progression of lesion volumes (baseline vs last follow-up, median, mL [IQR] 35.92 [16.20–57.93] vs 35.27 [14.98–55.33]; $p = 0.95$, n = 13, % of whole brain volume: 3.67 ± 2.29 vs 3.52 ± 2.47, $p = 0.59$, interval of median 3.26 years [range 0.91–9.52 years], figure 3D). This was confirmed by focused review of follow-up scans, which did not reveal involvement of additional white matter outside of territorial ischemic stroke lesions up to 10 years of follow-up (figure 3B).

One or multiple round to ovoid white matter CL (figure 4A) were detected in 16 patients (59.3%, maximum median n [IQR] 7.0 [0–25]) and increased over time (baseline vs last follow-up, median n [IQR] 3 [0–9] vs 10 [3–24]; n = 15, $p = 0.008$, figure 4, B–E).

Despite a shorter observation period and fewer patients (median years [IQR] 1.19 [0.87–2.94], n = 11), the overall findings were confirmed when only follow-up visits with identical scanner setups were included (data available from Dryad, table e-1, doi.org/10.5061/dryad.5x69p8d1f).

Ischemic Injury in Children and Young Adults: Large Artery Infarctions Affect Predominantly the Anterior Circulation

AIS lesions were present in 10 patients (37%, median lesion n, range 5, 1–16) with 46 lesions (82.1%) in the anterior circulation and 10 lesions (17.8%) in the posterior circulation (commonly in the posterior inferior cerebellar artery territory) (figure 5A). Four patients had acute features. Three

Table 1 Characteristics of Patients With *ACTA2* Arg179 Pathogenic Variants

	Median (range) or n (%)
Age at genetic diagnosis, y	4.0 (0.04–26.8)
Age at first scan, y	2.5 (0.01–31.5)
Age at last scan, y	7.2 (0.03–36.6)
Female sex	20 (74.0)
Vital status, deaths	4 (14.8)
Age at death, y	23 (0.5–32.7)
Causes of death	
Stroke complications	1 (25)
Aortic rupture	1 (25)
Pulmonary complications	1 (25)
Undetermined	1 (25)
Frequent neurologic symptoms	
Clinical seizures	8 (29.6)
Clinical symptoms of stroke	9 (33.3)
Headaches	5 (83)[a]
Mydriasis	17 (70.0)
Neurogenic bladder dysfunction	12 (44.4)
Imaging diagnosis of stroke	10 (37.0)
Age at stroke diagnosis, y	3.1 (0.25–31)
Cardiac risk factors	
PDA/APW	25 (92.6)
Age at PDA/APW closure surgery, y	0.17 (0.02–2.73)
Aortic aneurysm repair	4 (14.8)
Age at aortic aneurysm repair, y	12.3 (11.7–25.3)
Aortic dissection	5 (18.5)
Age at aortic dissection, y	14.5 (0.25–32.7)
Treatment	
Extracranial–intracranial bypass	5 (18.5)
Anticoagulants	5 (18.5)
Age at start, y	13.0 (4–24)
Antiplatelets	19 (70.3)
Age at start, y	4.0 (0.75–26)[b]
New stroke while on antithrombotic treatment initiation	3 (15.8)

Imaging marker	Baseline	Last follow-up	*p* Value
WMH, mL, median (IQR)	35.92 (16.20–57.93)	35.27 (14.98–55.33)	0.950
CL, median (IQR)	3 (0–9)	10 (3–24)	0.008

Continued

Table 1 Characteristics of Patients With *ACTA2* Arg179 Pathogenic Variants *(continued)*

Imaging marker	Baseline	Last follow-up	*p* Value
CS, median (IQR)	0 (0–3)	3.5 (0–4.25)	0.004
mCASS, median (IQR)	8.0 (4–13)	10.5 (6.25–20.25)	0.291
Rel ICA stenosis, mean (SD)	0.36 (0.14)	0.29 (0.10)	0.004

Abbreviations: AIS = ischemic stroke related to large artery occlusion; APW = pulmonary arterial hypertension; CL = cystic-like white matter lesions; CS = critical stenosis on time of flight magnetic resonance angiography; IQR = interquartile range; mCASS = modified focal Cerebral Arteriopathy of Childhood Severity Score; PDA = patent ductus arteriosus; Rel ICA stenosis = terminal to the petrous internal carotid artery diameter; WMH = white matter hyperintensities. Denominators may vary slightly due to missing data. Data are reported as median, raw quantiles, mean with SDs, or raw frequencies with weighted percentages.
[a] Dedicated headache evaluation was available for 6 patients over 2 years of age.
[b] Age starting antiplatelets is not specified for one patient.

patients (11.1%) had 1 or multiple sequential AIS lesions involving multiple territories during a 3–14 month follow-up period (figure 6). Nonacute ischemic infarctions related to small artery occlusion (lacunar lesions) were present but could not be quantified when not involving the gray matter due to the extent of white matter abnormalities.

Contrast-enhanced MRI was performed in 17 patients (62.9%, n = 34 scans). Four patients showed circumscribed enhancement of the cortical ribbon in the area of subacute infarction, but otherwise, no pathologic parenchymal or meningeal contrast enhancement was detected.

Figure 1 Infantile Vascular Abnormalities in Patients With *ACTA2* Arg179

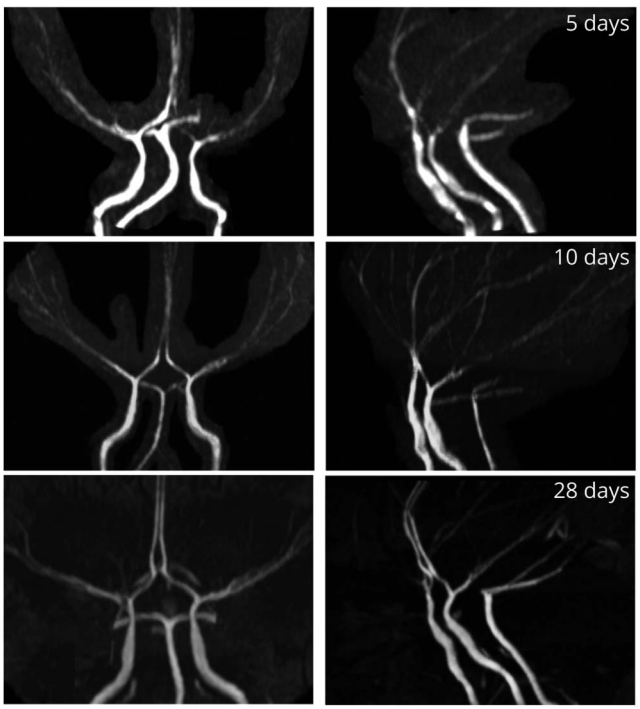

Maximum intensity projections of time of flight angiographies of 3 patients with *ACTA2* Arg179 pathogenic variant evaluated within the first month of life showing typical vessel abnormalities with intermittent changes in vessel caliber, short M1 segments of the middle cerebral arteries, and abnormal straight course of the basal cerebral arteries.

Hemorrhagic Parenchymal Injury is Uncommon and Limited to Microbleeds

Blood product sensitive imaging was available in 21 patients (77.8%, SWI:T2*W = 12:9). Only 2 patients had small (<3 mm) susceptibility artifacts consistent with microbleeds. One infant had a right periventricular microbleed and 1 child had 2 small right frontal lesions and 1 left frontal lesion. One patient had multiple susceptibility artifacts within a chronic large AIS lesion, which could represent secondary hemorrhage or calcifications. No large primary hemorrhagic lesions were observed. There was also no evidence of superficial siderosis indicative of remote subarachnoid or subpial hemorrhages.

Cerebral Artery Vasculopathy is Progressive and Predictive of AIS

TOF MRAs were available in 26 patients with SMDS, 15 of which had follow-up MRAs. Major cerebral artery abnormalities were observed in all patients. The most prominent and constant feature was an abnormal straight course of the intracranial carotid artery (ICA; losing its S shape in the cavernous sinus) and between the terminal portion of ICA and the distal segments of the middle, anterior, and posterior cerebral arteries (figure 7). A transition from dilation of the petrous ICA to stenosis of its distal cavernous sinus and supraclinoid segments (terminal ICA), where the vessel wall transitions from elastic to muscular anatomy, was present in all patients. The ratio between diameters of the terminal ICA and its proximal ipsilateral petrous portion was found reduced by 50% or higher in 23/26 patients. Only 4 patients under 2.8 years of age showed ratios comparable to age-matched controls. These ICA caliber abnormalities were progressive over time in 12 of the 15 patients (80%) with available follow-up MRAs (figure 7A).

Compared to controls, significantly lower mean ICA tortuosity indices and mean ICA–MCA angles were found in patients with *ACTA2* Arg179 pathogenic variants (n = 9 *ACTA2* Arg179 vs n = 5 controls, mean ± SD 1.31 ± 0.12 vs 1.57 ± 0.15; $p = 0.004$ and 125.1° ± 11.9° vs 139.6° ± 7.6°; $p = 0.031$, respectively, figure 7B). The automatically measured

diameters and ratios correlated well with the manual quantifications (r = 0.78, 95% confidence interval 0.24–0.95, 2-tailed p = 0.013).

Critical stenosis of the cerebral arteries (ICA, M1, M2, M3, A1, A2, P1, P2, P3 segments) was present in 11 of the 26 patients (42.3%, figure 5B). Nine of these patients showed increased numbers of CS over time, 1 was stable, and 1 lacked follow-up imaging to allow determination of progression (figure 5, B and C). Anterior and middle cerebral arteries were most frequently affected. The semiquantitative mCASS scoring did not capture significant progression over time (baseline vs last follow-up, median mCASS [IQR] $8.0^{4–13}$ vs 10.5 [6.25–20.25]; p = 0.29, n = 15).

Increased tortuosity with a corkscrew appearance was observed in smaller and more distal arterial branches in 13 of 26 patients. This was limited to 3 or fewer large artery territories in 7 patients and more diffuse in 6 patients (figure 5D).

In 20 patients older than 1.15 years who had both parenchymal and vascular imaging available for comparison, we found that a decrease in the terminal/petrous ICA ratio correlated with higher numbers of CS (r_p = −0.629, p = 0.003) and presence of CL (r_{pb} = −0.571, p = 0.009), while no significant correlation with WMH was found (r_p = −0.217, p = 0.359). In a multivariable model (including age, WMH, numbers of CL and CS, and presence of cardiac emboli source), the relative stenosis of the terminal to petrous ICA was the only independent predictor of having had AIS (acute or chronic lesions, pseudo R^2 = 0.5, p < 0.029, n = 26; table 2) and a logistic regression indicated that patients with a relative terminal ICA stenosis of >0.7 (terminal/petrous ICA ratio <0.3) are highly likely to have had AIS (acute or chronic based on lesion imaging characteristics, yes vs no, $x^2[1] = 12.28$, p < 0.001; n = 26, figure 5E).

Figure 2 Infantile Parenchymal Abnormalities in Patients With *ACTA2* Arg179

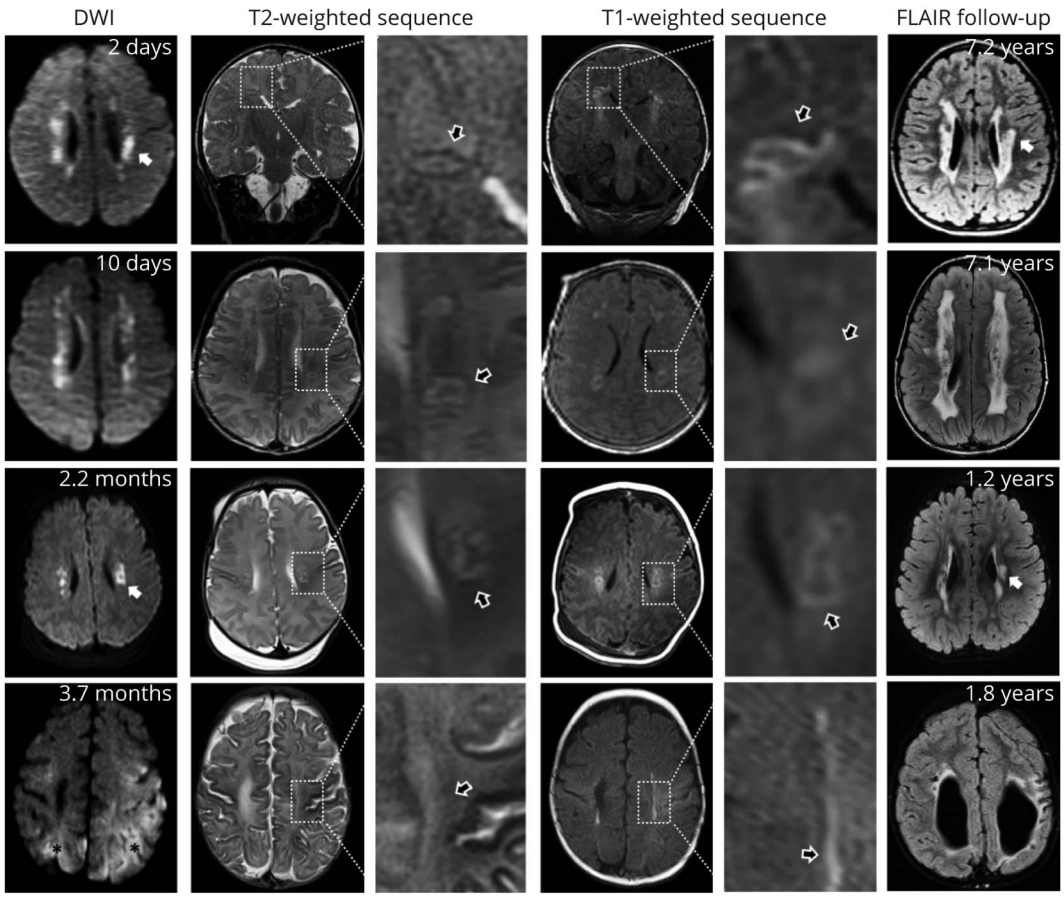

Diffusion-weighted imaging (DWI) and T2- and T1-weighted (T2W, T1W) sequences of 4 patients with *ACTA2* Arg179 pathogenic variants aged 2, 10, 66, and 110 days. Right: Follow-up fluid-attenuated inversion recovery (FLAIR) sequences of the same patients of each row at 7.2, 7.1, 1.2, and 1.8 years of age. All patients show acute DWI lesions consistent with internal border zone infarctions. White matter corresponding to acute DWI lesions shows T2W-hypointense and T1W-hyperintense, mostly ring-like signal abnormalities (black arrows). Note highlighted similar shapes of the edges of acute DWI lesions and of long-term follow-up white matter hyperintensities on FLAIR sequences (white arrows). The patient in row 4 had additional hemodynamic ischemic strokes (black asterisks) due to complications during heart surgery in addition to deep white matter lesions.

Figure 3 White Matter Hyperintensity Lesions in Patients With *ACTA2* Arg179

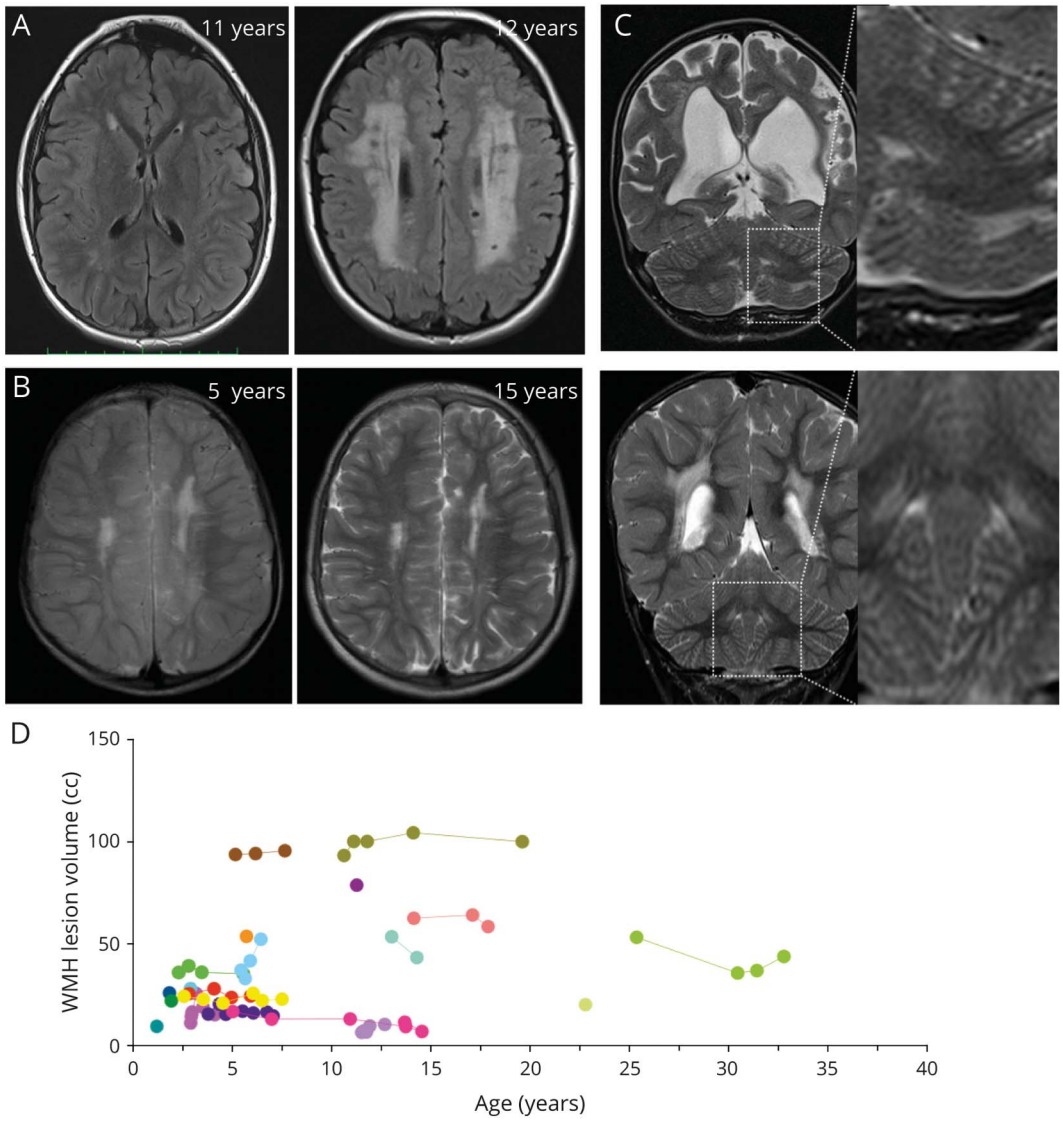

A) Representative fluid-attenuated inversion recovery (FLAIR) images to illustrate the range of white matter hyperintensities (WMH) from limited to extensive found in *ACTA2* Arg179 patients. Both patients are between 11 and 12 years of age. (B) Representative T2-weighted images of a 5-year-old boy and corresponding follow-up visit 10 years later showing stable extent of WMH burden. (C) Representative T2-weighted sequence to illustrate periventricular and subcortical cerebellar WMH infrequently found in *ACTA2* Arg179 patients. (D) Individual longitudinal data on WMH.

Imaging Findings Do Not Differ Between Sex or the Arginine 179 Substituting Amino Acid

p.Arg179Cys substitution was less common than p.Arg179His substitution in our cohort. On average, the p.Arg179Cys patients were not significantly different in age but showed a trend towards higher WMH volumes when compared with p.Arg179His mutations (p.Arg179Cys vs p.Arg179His; median years [IQR] 0.49 [0.027–10.59] vs 2.86 [0.005–31.57]; p = 0.45, WMH median mL [IQR] 53.55 [25.22–97.68] vs 22.89 [14.98–78.62]; p = 0.07). No significant differences were found regarding the presence of numbers of AIS, CL, or CS between mutations (table 3).

A binominal test indicated that the proportion of male patients (0.26) was lower than expected for a de novo mutation that should occur equally in males and females (vs 0.51, p = 0.007, 1-tailed). Comparison of female and male sex showed no significant differences in parenchymal lesion burden or numbers of arterial abnormalities (data available from Dryad, table e-2, doi.org/10.5061/dryad.5x69p8d1f).

Discussion

Our systematic analysis of this retrospective cranial MRI cohort of patients with SMDS due to *ACTA2* Arg179 pathogenic variants yield (1) the natural history of white matter lesions, (2) characteristic patterns in young infants of intracranial vasculopathy and acute ischemic injury, (3) a correlation between terminal ICA and cerebral arteries stenosis and arterial ischemic infractions, and (4) a clinically applicable

Figure 4 Cyst-Like White Matter Lesions in Patients With *ACTA2* Arg179

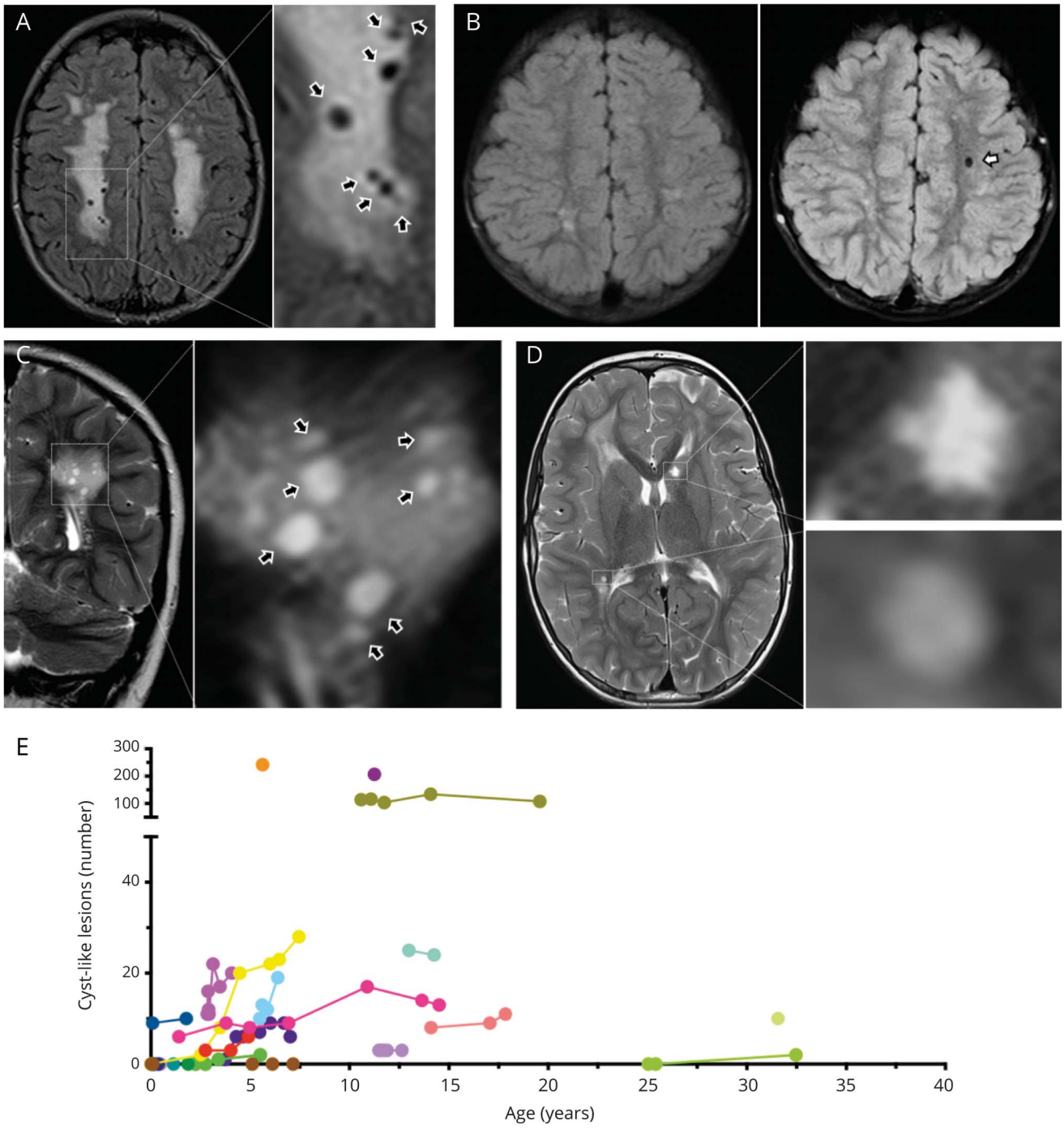

Upper row shows fluid-attenuated inversion recovery (FLAIR)-weighted, lower row shows T2-weighted images to illustrate CSF-like signal intensity of cyst-like white matter lesions (CL). (A) Magnification of multiple CLs (black arrows). (B) Baseline (left) and 3-year follow-up (right) of the same *ACTA2* Arg179 patient to illustrate emergence of an additional CL in the left frontal white matter (white arrow). (C) Same patient as in A. Coronal imaging illustrates round to ovoid shape of CL (black arrows) in a different plane. (D) Magnifications to illustrate differences of CL and lacunes. The lesion in the right peritrigonal white matter was classified as a CL based on a smooth edge and round shape. In contrast, the star-shaped, irregularly edged lesion in the left caudate head was considered a lacune of presumed vascular origin. (E) Individual longitudinal data on numbers of CL.

diagnostic tool to monitor progression of ICA vasculopathy since early infancy.

Our analysis of WMH revealed abnormalities ranging from minimal periventricular hyperintensities to diffuse deep white matter and subcortical involvement. Overall these lesions showed stable volumes over time and match areas of acute ischemic injury found in early infancy. Evidence of small vessel disease was also suggested by white matter lacunar infarcts and in the gray matter of the basal ganglia and thalami.

Figure 5 Vascular Lesions in Patients With *ACTA2* Arg179

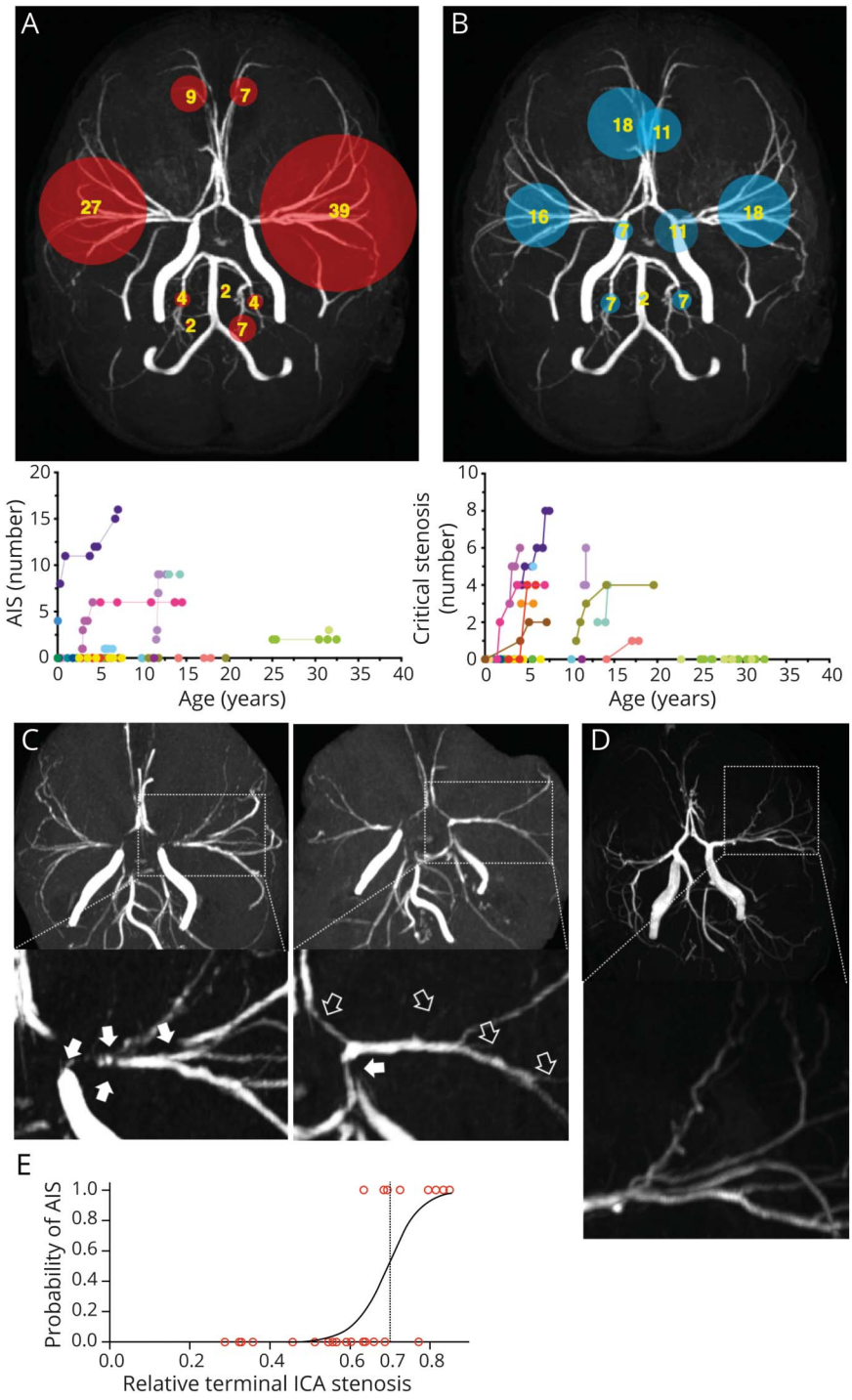

A) Frequencies of involved vascular territories of ischemic strokes related to large artery occlusion (AIS) and longitudinal data on numbers of AIS. (B) Frequencies of critical stenosis (CS) within the vascular territories and longitudinal data on number of CS. Numbers in circles indicate percentage of total lesions detected in the cohort. Circle size is proportional to lesion frequency. (C) Representative magnifications of maximum intensity projections of time of flight angiographies (TOF MIP) of the same patient illustrating the emergence of new CS defined as short segmented or wide-stretching signal loss following the vessels course from baseline (white arrows) to follow-up (black arrows). (D) Magnifications of TOF MIP illustrating corkscrew appearance of cerebral vessels found frequently in patients with *ACTA2* Arg179 pathogenic variants. (E) Logistic regression curve representing an estimate of the probability for AIS depending on the relative terminal internal carotid artery (ICA) stenosis.

A previous study demonstrated that areas of WMH correspond microscopically to rarefaction of the periventricular neuropil and axonal damage, findings most consistent with chronic ischemic injury.[14]

Bilateral deep white matter acute ischemic lesions were found in infants (<6 months) without evidence of concomitant significant stenosis of the large and medium-sized cerebral arteries. These lesions corresponded with border zone areas between cerebral artery territories known to have the highest vulnerability to reduced cerebral perfusion due to their low vessel density and lack of collateral circulation (also known as internal watershed).[4,15] We hypothesize that poor cerebrovascular autoregulation due to vascular smooth muscle dysfunction predisposes infants with SMDS to deep watershed infarctions when episodes of hypotension/hypoxia occurred

Figure 6 Infarct Progression in a Patient With *ACTA2* Arg179

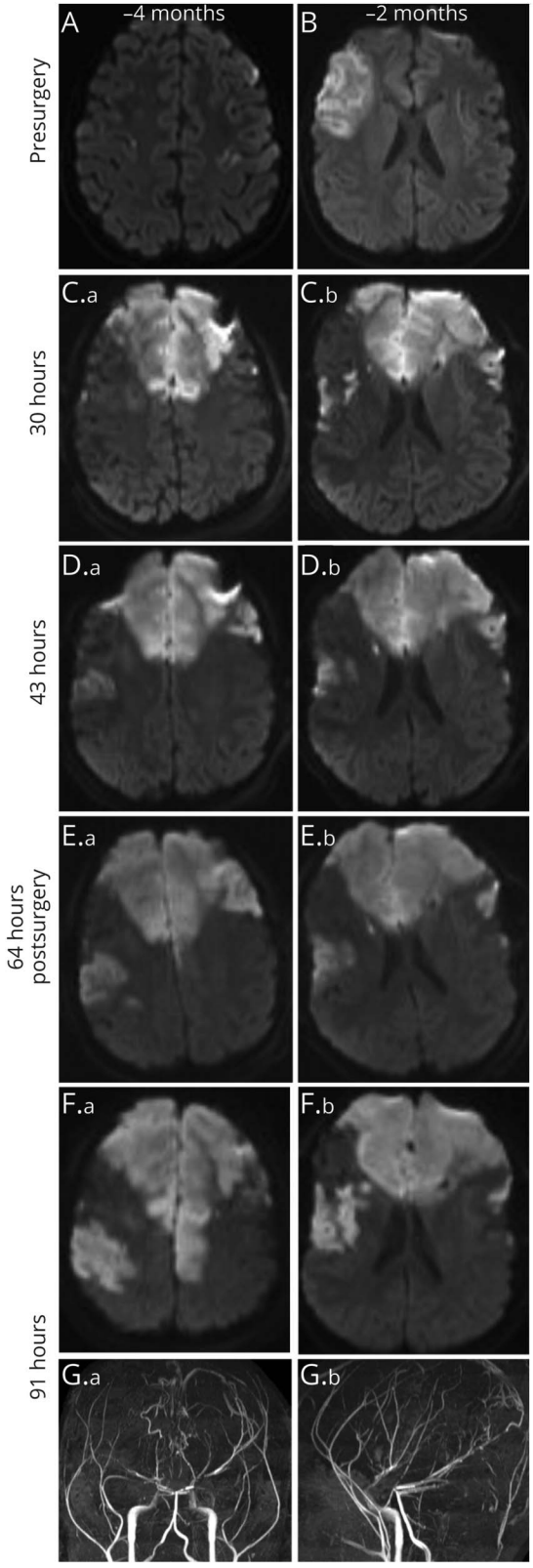

Diffusion-weighted imaging of an 11-year-old girl with *ACTA2* p.Arg179His mutation before (A, B) and after (C–F: 30, 43, 64, and 91 hours postsurgery) and time of flight angiographies after (G: 91 hours postsurgery) revascularization surgery with bilateral superficial temporal artery to pial synangiosis illustrating the presence of ischemic strokes and rapid progression of infarcts over time postsurgery.

during labor, anesthesia, acute respiratory distress, pulmonary artery hypertension, or right-to-left shunting from large patent ductus arteriosus or aorto-pulmonary windows.

Additional white matter abnormalities in these patients included cystic-like lesions, which can be distinguished from observed lacunar infarcts by their smooth regular margin appearance in most cases (figure 4D). A key imaging feature associated with lacunes of presumed vascular origin—a T2W/FLAIR-hyperintense rim—cannot be reliably detected in CL within hyperintense white matter areas, therefore a proportion of the lesions rated as CL could be lacunar infarcts. It is unclear whether CL represent focally enlarged perivascular spaces or ischemic cystic rarefaction of the white matter.[14,16] Their distinct appearance and correlation with progressive large artery steno-occlusive vasculopathy suggests that chronic hypoperfusion and disturbances in CSF pulsation could be underlying mechanisms.

While deep white matter lesions appeared in all patients in infancy, arterial ischemic infarcts involving white and gray matter were identified only after 2.85 years of age with the exception of one patient who had intraoperative aortic dissection, severe hypovolemia, and anoxic injury at 3 months of age (patient 4 in figure 2). Hypothesized etiology for AIS include the above-mentioned hypotensive events and suspected thromboembolism from prosthetic aortic valves in the adult patient with suspended anticoagulation for a diagnostic procedure. In addition, serial imaging on a 6-year-old patient during the evolution of an acute ischemic stroke (figure 6) showed contiguous expansion of ischemia across arterial territories over hours. This atypical pattern of ischemic injury spread illustrated the severe limitation of collateral recruitment commonly achieved by arteriolar vasodilation to salvage tissue at risk of infarction (penumbra).[17] In contrast to other progressive arteriopathies, patients with *ACTA2* Arg179 pathogenic variants lack the classic moyamoya-like basal collateral vessels.[4] Whether these mutations reduce angiogenesis and ability to form collaterals remains to be determined as lack of contrast-enhanced MRA limited our ability to investigate this relevant question.

With regards to large vessel vasculopathy, our study revealed that dilation of the petrous and cavernous segments of the ICA and straightening of cerebral arteries are present as early as 2 days of life and a comparison with a pediatric stroke control cohort without vasculopathy confirmed the severity of these abnormalities (figure 7). However, stenosis of the terminal ICA and cerebral artery only appeared after the third year of life. Limited histopathology of cerebral arteries in patients with SMDS has shown neointimal cellular hyperplasia and thickening of medial layer with increased collagen deposition, which could account for their luminal stenosis.[14] For the first time, we report a relationship between stenosis and ischemic injury as number of CS in a given cerebral artery coincided with AIS of their territory. The previously described focal Cerebral

Figure 7 Cerebral Artery Vasculopathy Is Progressive in Patients With *ACTA2* Arg179

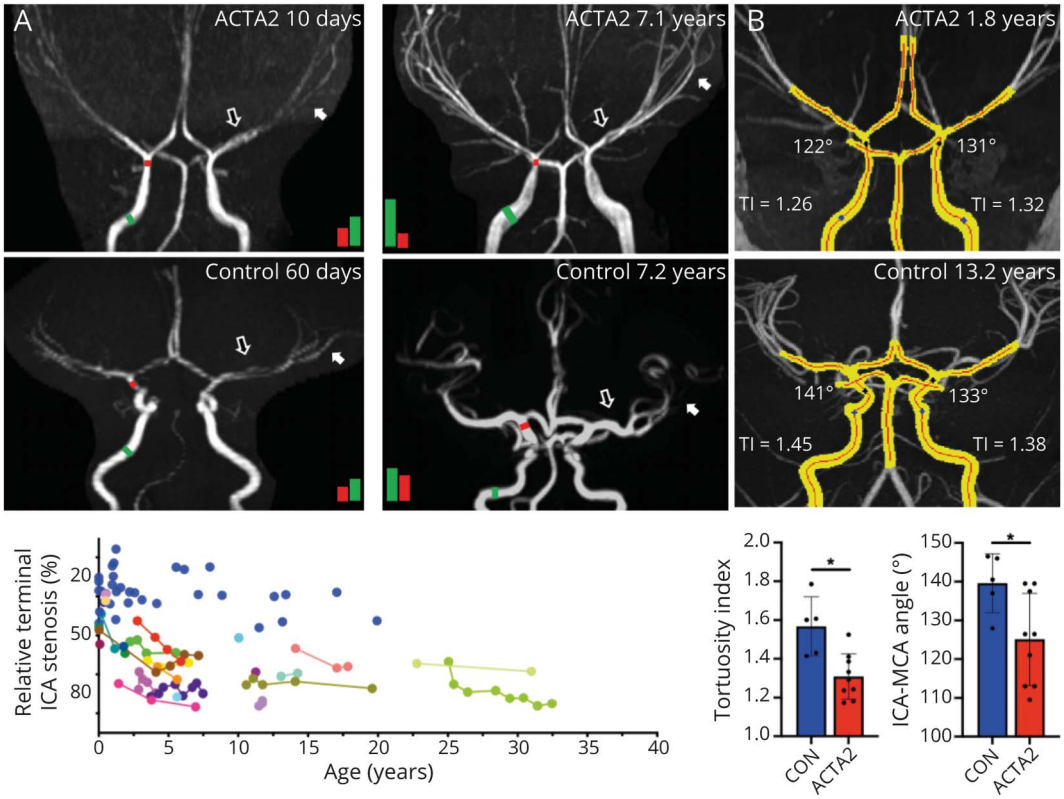

A) Segmented maximum intensity projections (MIPs) of an *ACTA2* p.Arg179His patient and a patient with pediatric stroke without vasculopathy (control). The red line is the automatically generated centerline. Tortuosity index (TI) is labeled of each internal carotid artery (ICA), and the angle of incidence between the ICA and middle cerebral artery (MCA). Below are controls vs *ACTA2* Arg179 patients for mean TI and mean ICA–MCA angles. *$p < 0.05$. (B) Baseline at 10 days (left) and follow-up at 7.1 years (right) of a patient with *ACTA2* p.Arg179Cys pathogenic variant compared to a 60-day-old (left) and a 7.2-year-old (right) control patient. Black and white arrows indicate abnormal straight appearance of basal cerebral arteries that persists in aging in *ACTA2* Arg179 patients. Colored bars are proportional to the quantified diameter of the terminal (red bar) to the petrous ICA (green bar) and illustrate age-related progressive stenosis determined by their ratio. Diagram illustrates individual longitudinal data on relative terminal to petrous ICA stenosis. Blue dots represent control patients.

Arteriopathy of Childhood Severity Score[4] underestimated number of stenosis in SMDS and its modification to include steno-occlusive lesions beyond the M2 and A2 segments and in the posterior circulation was not able to detect disease progression (figure 5C).[12]

Notably, narrowing of the terminal ICA (terminal/petrous ICA diameters) reliably correlated with AIS and could offer a robust biomarker for measuring disease progression before stroke onset. This normalized measurement was highly reproducible (intraclass correlation coefficient 0.96) and could be easily applied in the clinical setting. Moreover, net increase in flow velocities caused by the ICA stenosis could be assessed by noninvasive transcranial Doppler ultrasound (TCD) and become a valuable biomarker to monitor early steno-occlusive disease progression.

It is unclear why the anterior circulation is more frequently involved. Histopathology studies showed lesser intima thickness on arteries of the posterior circulation.[14] The lower wall shear stress of the vertebrobasilar system due to its anatomy and distance from the left ventricular outflow tract may be protective for the development of stenosis. Conversely, aneurysmatic dilation of the ascending aorta and elastic portions of the ICA with loss of its curvature in the cavernous sinus could lead to higher wall shear stress and stenosis in the anterior circulation.

Other notable patterns of arteriopathy in this cohort included increased involvement of anterior circulation arteries, a finding that corresponds with 2 previous studies of *ACTA2* Arg179,[1,14] and increased tortuosity of distal smaller branches taking off from their abnormally straightened parent cerebral basal arteries in approximately half of patients. Similarly, retinal artery branches are commonly highly tortuous, corkscrew-like in patients with these mutations.[18]

Despite a higher number of p.Arg179His mutations and female patients, our analysis revealed no significant differences in their parenchymal lesion burden or basal artery characteristics. The disproportionally low number of male patients for an autosomal dominant disease suggests that males go undiagnosed either due to a less characteristic or more severe phenotype leading to death before genetic testing.

Table 2 Multivariable Analysis for Risk of Ischemic Stroke (Acute or Chronic)

	OR	95% CI	*p* Value
Age, for each year increase	0.991	0.786–1.199	0.387
Cardiac emboli source,[a] yes vs no	0.323	0.003–13.71	0.563
WMH, for each mL increase	0.976	0.878–1.025	0.387
CL, for each no increase	1.005	0.984–1.032	0.8306
Rel ICA stenosis, for each % increase	1.223	1.061–1.621	0.0438
CS, for each no increase	1.045	0.553–1.847	0.880

Abbreviations: CI = confidence interval; CL = cystic-like white matter lesions; CS = critical stenosis on time of flight magnetic resonance angiography; OR = odds ratio; Rel ICA stenosis = terminal to the petrous internal carotid artery diameter; WMH = white matter hyperintensities.
[a] Cardiac emboli sources excluded patent ductus arteriosus or aorto-pulmonary window because this was present in over 92% of patients.

Limitations of this study include disease rarity, unsystematic follow-up intervals, and nonstandardized scanning parameters. Over the years, data were collected with improving imaging technology and higher sensitivity to quantified lesions. This could have introduced bias in the longitudinal analysis. In addition, same patients were not always scanned with an identical scanner setup (including 3.0T vs 1.5T MRI systems). An analysis of imaging markers for those patients imaged on an identical scanner setup confirmed our overall findings.

Referral bias is likely since all patients in this cohort were initially MRI scanned because of concerns of neurologic injury (due to symptoms or suspected SMDS) and the proportion of follow-up imaging due to symptoms is unknown to us.

Our data strongly suggest that white matter injury can occur early during infancy and while WMH appeared stable during the available observation period, it is unclear how these lesions affect global brain development and growth. Morphologic brain abnormalities such as flattening of the pons and a mildly hypoplastic posterior corpus callosum previously described in *ACTA2* mutations in patients >10 years of age[9] were found in all infants of this cohort. The frequent presence of white matter lesions at young age warrants further studies to distinguish abnormalities in global brain development from those secondary to tissue injury. However, available scans were insufficient for more in-depth analysis of white and gray matter volumes.

Based on our data, the presence of white matter injury and significant large and medium cerebral artery stenosis around the age of 3 years warrants baseline MRI screening within the first 2 years to guide early developmental interventions or initiation of platelets antiaggregation for primary or secondary

Table 3 Characteristics of p.Arg179His vs p.Arg179Cys *ACTA2* Patients

	p.Arg179His (n = 19)	p.Arg179Cys (n = 7)	*p* Value
Age at baseline, y	2.9 (0.005–31.57)	0.5 (0.027–10.59)	0.45
Age at last presentation, y	7.5 (0.013–32.47)	5.6 (0.49–19.58)	0.42
Female	14 (70)	6 (85.7)	1.00
WMH, mL	22.89 (14.98–78.62)	53.55 (25.22–97.68)	0.07
Number of AIS	0 (0–5)	0 (0–0.25)	0.15
Number of CL	3 (0–22)	8.5 (4.5–141.5)	0.31
Number of CS	0 (0–3.5)	3 (0–4)	0.41
Number of mCASS	8 (3–21)	6 (1–18)	0.27
Rel ICA stenosis	0.33 (0.15)	0.45 (0.20)	0.16

Abbreviations: AIS = ischemic stroke related to large artery occlusion; CL = cystic-like white matter lesions; CS = critical stenosis on time of flight magnetic resonance angiography; mCASS = modified focal Cerebral Arteriopathy of Childhood Severity Score; Rel ICA stenosis = terminal to the petrous internal carotid artery diameter; WMH = white matter hyperintensities.
Denominators may vary slightly due to missing data regarding mutation in 1 patient. Data are reported as median (range), raw quantiles, mean (SD), or raw frequencies (weighted percentages).

stroke prevention. However, frequency and duration of MRI scanning must be balanced against the risk of episodic low blood pressure and cerebral hypoperfusion associated with induction of anesthesia necessary for comprehensive studies in young children. When available, TCD and fast nonsedated MRI protocols with TOF MRA are good alternatives to monitor early disease progression and timing of interventions. New neurologic symptoms and a high pretest probability of changing management should drive indication for imaging studies.

Antithrombotic drug treatment was frequently initiated at varying times in the medical history of patients, hampering our ability to evaluate its effects on stroke prevention and other evaluated neuroimaging biomarkers. Systematic investigations in a prospective manner will be needed to understand risks and benefits of antithrombotic therapy and cerebral revascularization surgery. Our data illustrating the low incidence of hemorrhage in these patients suggests that pathogenic variants of *ACTA2* Arg179 do not increase risk of intracranial bleeding even if exposed to long-term antiaggregant or therapeutic anticoagulation, an important observation when assessing safety of these treatments needed during surgical procedures and stroke prevention.

We found early, characteristic, quantifiable, and progressive cerebral lesion patterns related to large and small vessel disease in patients with *ACTA2* Arg179 pathogenic variants. Our longitudinal data suggest parenchymal injury results from cumulative ischemic injury associated with small vessel disease, steno-occlusive vasculopathy, and hypoperfusion during hemodynamic decompensations or thromboembolic cerebral artery occlusions. We also observed a unique pattern of subacute lesion propagation that can follow arterial ischemic strokes reflective of severe loss of cerebrovascular autoregulation. The evaluated metrics can be used for early diagnosis at birth and to monitor disease progression and response to pharmacologic or surgical interventions. Future prospective longitudinal studies are needed to better characterize the contribution of triggers and risk factors associated with progression of cerebral disease.

Acknowledgment

The authors thank the families and their respective local care providers for their participation in this study; and the newly founded *ACTA2* Alliance Foundation for the research advocacy, education, and support provided to families affected by this disease.

Study Funding

This study was supported by NIH R01 HL109942, an American Heart Association Merit Award, and the Temerty Family Foundation (D.M.M.) and by NINDS K08 NS094683-01 (P.L.M.).

Disclosure

The authors report no disclosures relevant to the manuscript. Go to Neurology.org/N for full disclosures.

Publication History

Received by *Neurology* February 29, 2020. Accepted in final form September 11, 2020.

Appendix Authors

Authors	Location	Contribution
Arne Lauer	Goethe University, Frankfurt aM, Germany	Study concept and design, analysis and interpretation of data, and drafting of the manuscript
Samantha L. Speroni	Massachusetts General Hospital, Harvard Medical School, Boston	Data collection, analysis and interpretation of data, and drafting of the manuscript
Jay B. Patel	Massachusetts General Hospital, Harvard Medical School, Boston	Data collection and critical revision of the manuscript for important intellectual content
Ellen Regalado	McGovern Medical School, University of Texas Health Science Center at Houston	Data collection and revising the manuscript
Myoung Choi	Goethe University, Frankfurt aM, Germany	Data collection and revising the manuscript
Edward Smith	Boston Children's Hospital, Harvard Medical School, MA	Critical revision of the manuscript for important intellectual content
Jayashree Kalpathy-Kramer	Massachusetts General Hospital, Harvard Medical School, Boston	Critical revision of the manuscript for important intellectual content
Paul Caruso	Massachusetts General Hospital, Harvard Medical School, Boston	Data collection and revision of the manuscript
Dianna M. Milewicz	McGovern Medical School, University of Texas Health Science Center at Houston	Data collection and critical revision of the manuscript for important intellectual content
Patricia L. Musolino	Massachusetts General Hospital, Harvard Medical School, Boston	Study concept and design, analysis and interpretation of data, drafting of the manuscript, and study supervision

References

1. Milewicz DM, Kwartler CS, Papke CL, Regalado ES, Cao J, Reid AJ. Genetic variants promoting smooth muscle cell proliferation can result in diffuse and diverse vascular diseases: evidence for a hyperplastic vasculomyopathy. Genet Med 2010;12:196–203.
2. Meuwissen MEC, Lequin MH, Bindels-de Heus K, et al. *ACTA2* mutation with childhood cardiovascular, autonomic and brain anomalies and severe outcome. Am J Med Genet A 2013;161A:1376–1380.
3. Regalado ES, Mellor-Crummey L, Backer J, et al. Clinical history and management recommendations of the smooth muscle dysfunction syndrome due to *ACTA2* arginine 179 alterations. Genet Med 2018;20:1206–1215.
4. Munot P, Saunders DE, Milewicz DM, et al. A novel distinctive cerebrovascular phenotype is associated with heterozygous Arg179 *ACTA2* mutations. Brain 2012; 135:2506–2514.
5. Milewicz DM, Østergaard JR, Ala-Kokko LM, et al. De novo *ACTA2* mutation causes a novel syndrome of multisystemic smooth muscle dysfunction. Am J Med Genet A 2010;152A:2437–2443.

6. Amans MR, Stout C, Fox C, et al. Cerebral arteriopathy associated with Arg179His *ACTA2* mutation. BMJ Case Rep 2013;2013:bcr2013010997.
7. Cuoco JA, Busch CM, Klein BJ, et al. *ACTA2* cerebral arteriopathy: not just a puff of smoke. Cerebrovasc Dis 2018;46:161–171.
8. Masuoka T, Hayashi N, Hori E, Kuwayama N, Ohtani O, Endo S. Distribution of internal elastic lamina and external elastic lamina in the internal carotid artery: possible relationship with atherosclerosis. Neurol Med Chir 2010;50:179–182.
9. D'Arco F, Alves CA, Raybaud C, et al. Expanding the distinctive neuroimaging phenotype of *ACTA2* mutations. AJNR Am J Neuroradiol 2018;39:2126–2131.
10. Wardlaw JM, Smith EE, Biessels GJ, et al. Neuroimaging standards for research into small vessel disease and its contribution to ageing and neurodegeneration. Lancet Neurol 2013;12:822–838.
11. Chen YW, Gurol ME, Rosand J, et al. Progression of white matter lesions and hemorrhages in cerebral amyloid angiopathy. Neurology 2006;67:83–87.
12. Fullerton HJ, Stence N, Hills NK, et al. Focal cerebral arteriopathy of childhood: novel severity score and natural history. Stroke 2018;49:2590–2596.
13. Wei F, Diedrich KT, Fullerton HJ, et al. Arterial tortuosity: an imaging biomarker of childhood stroke pathogenesis?. Stroke 2016;47:1265–1270.
14. Georgescu M-M, Pinho MdC, Richardson TE, et al. The defining pathology of the new clinical and histopathologic entity *ACTA2*-related cerebrovascular disease. Acta Neuropathol Commun 2015;3:81.
15. Mangla R, Kolar B, Almast J, Ekholm SE. Border zone infarcts: pathophysiologic and imaging characteristics. Radiographics 2011;31:1201–1214.
16. Mestre H, Kostrikov S, Mehta RI, Nedergaard M. Perivascular spaces, glymphatic dysfunction, and small vessel disease. Clin Sci 2017;131:2257–2274.
17. Koga M, Reutens DC, Wright P, et al. The existence and evolution of diffusion-perfusion mismatched tissue in white and gray matter after acute stroke. Stroke 2005;36:2132–2137.
18. Moller HU, Fledelius HC, Milewicz DM, Regalado ES, Ostergaard JR. Eye features in three Danish patients with multisystemic smooth muscle dysfunction syndrome. Br J Ophthalmol 2012;96:1227–1231.